One-shot detection limits of time-alignment two-photon illumination radar

Wen-Long Gao(高文珑)[1], Lu-Ping Xu(许录平)[†], Hua Zhang(张华)[‡], Bo Yan(阎博), Peng-Xian Li(李芃鲜), and Gui-Ting Hu(胡桂廷)

School of Aerospace Science and Technology, Xidian University, Xi'an 710126, *China*

(Received 16 August 2022; revised manuscript received 29 October 2022; accepted manuscript online 3 November 2022)

Quantum radar has recently gained increasing importance in a number of military applications. The estimation accuracy of one-shot quantum illumination events is significant in target detection. However, the accuracy is inevitably deteriorated by measurement noises. The traditional one-shot illumination emits a single photon towards a certain area which thermal noise exists in the path to, and the states of the received photons are hard to distinguish in the following processing. Therefore, a new optical probe source is proposed in this work. The independent detecting unit in the enhanced illumination is comprised of two photons aligned in time by using Hong–Ou–Mandel (HOM) interferometer. Further, one-shot detection in a general discrete model is realized and it proves a significant promotion in accuracy. The expansion of useful parts in parameter space and the lower minimal error probability for hypothesis testing have been mathematically demonstrated. The accuracy of one-shot detection can be effectively improved by the proposed scheme implying that it possesses great potential applications in quantum illumination and imaging.

Keywords: quantum information, quantum optics, photonic

PACS: 03.67.–a, 03.67.Mn, 42.55.Tv **DOI:** 10.1088/1674-1056/ac9fc3

1. Introduction

Finding the optimal probe scheme for illumination is one of the most critical tasks in the field of quantum radar. At present, the problems restricting the development of quantum radar are that the optical signal sources is not bright enough, atmospheric scattering, and absorption of the target, so the radar receiver can obtain few useful signal photons. In addition, it is necessary to identify the emitted signal photons and various material factors from the complex environmental noises, all the above factors prevent the practical application of quantum radar from maturing. As an important type of quantum radar, quantum illumination has a simple application architecture and is suitable for several different illumination sources. The accuracy of radar detection can be effectively improved through various quantum methods.[1–4] Therefore, the illumination source, noise influence, and measurement methods in quantum illumination have become a research hotspot. In particular, the design of illumination sources has important application, and their performance analysis has been completed recently, and many experiments have been successful.[5–9] While in the whole radar system, the quantum state emitted by the transmitter and the quantum measurement at the receiver need optimizing. On this basis, the performance limit of the quantum illumination state in the detection needs determining mathematically, and clear derivation results must be given. The one-shot measurement is the smallest unit event in illumination radar, and its detection performance under various kinds of illumination sources has the important significance in the radar detection system.[10] As a consequence, it is a research hotspot of quantum radar to find an illumination source that can improve the performance in one-shot illumination and can be prepared experimentally. The pursuit of wider target applicability and lower minimum error probability in one-shot detection also paves the way for the experimental landing of quantum radar.

Plenty of efforts were made to seek for a high-brightness and well-controlled optical transmitter.[11,12] Hereinto, an effective method of producing particular photon states and controlling their specific quantum properties has matured considerably, by the spontaneous parametric down-conversion (SPDC) process in well-prepared nonlinear crystals.[13,14] This SPDC process was predicted in the 1960s,[15] and first demonstrated experimentally by Burham and Weinberg in 1970.[16] Until now, the most mature and widely used nonlinear crystals have been BBO (BaB_2O_4),[6] KDP (KD_2PO_4),[17] and PPKTP (periodically poled $KTiOPO_4$).[18] Based on two types of SPDC processes in several nonlinear crystals, photon pairs with different characteristics can be prepared experimentally and steadily.[19,20] Meanwhile, to reach better performance, various quantum resources such as entanglement[21] and squeezing[22] were applied to quantum computation,[23,24] quantum cryptography,[25] quantum simulation,[26,27] quantum teleportation,[28] quantum metrology,[29,30] *etc*. Most of the investigations in the field of quantum measurement tend to improve the resolution and signal-to-noise ratio (SNR) of the

[†]Corresponding author. E-mail: Lpxu@mail.xidian.edu.cn
[‡]Corresponding author. E-mail: zhanghua@mail.xidian.edu.cn

© 2023 Chinese Physical Society and IOP Publishing Ltd

receiver,[31–33] which exactly manifests the particular advantages for quantum resources over conventional measurement. Actually, increasing either the number of photons in pulses or the detection times in ranging events helps improve the precision of positioning procedures, and so does it in entangled and squeezed pulses.[34–36] Generally, the two photons produced by the pump photon are utilized separately by dividing their paths into different spatial paths, and subsequently, a joint positive-operator valued measure (POVM) measurement is performed on these two paths at the receiver.[37] More importantly, the scheme of quantum entangled illumination proposed by Lloyd has exhibited explicit advantages in SNR over conventional illumination.[38] This method which can increase the SNR of the radar receiver primarily depends on the dimension of entanglement even if noises and losses are huge,[31,39,40] and was later realized in the experiment by Lopaeva *et al.*[41] The error probability analysis in the above-mentioned illumination process has also matured with the efforts of many scholars.[42] Recently, Yung *et al.* conducted the detailed analyses of quantum entanglement advantages in terms of the minimum error probability of hypothesis testing at the receiver for the one-shot event.[10] Construction of hypothesis testing problem aims to identify whether the object is absent or not by treating it as a problem of channel discrimination, where there exist the two channels: one corresponds to the presence of the target, and the other corresponds to the absence of the target.[43–49] Thereinto, the white noise and arbitrary noise situations for conventional and entangled illumination have been discussed, and crucial conclusions were obtained.[50,51] Even more importantly, an accurate and reliable framework was also provided for analyzing the performance of one-shot quantum illumination.[10] Based on the framework above, the primary target of one-shot illumination then turns to investigating how can we optimize the probe scheme to make these two channels most discriminable.

However, conventional radars still have shortcomings in target detection such as poor accuracy and resolution.[52–54] Meanwhile, disturbances like false alarm detections and miss detections are mainly caused by measurement noises and ghost waves. Therefore, unlike previous researches, we attempt to explore the quantum advantages of simultaneous detection of two-photon to reduce these disturbances as much as possible. Besides, the time and spatial correlation characteristics of two-photon have also great potential applications in imaging and positioning.[55] Considering that the temporal correlation of photons in the two output paths of the SPDC procedure is easily affected by the length of fiber realistically, we determine to calibrate the two optical paths for time via the Hong–Ou–Mandel (HOM).[17] effect and take both two arms of the interferometer output as the transmitting port of radar. The down-converted identical two photons with a fixed and small enough time interval can be regarded as a larger detection unit in the illumination process. We analyzed its minimal error probability performance in one-shot detection and obtained an effective performance improvement. On the premise that probe state and POVM measurement are both optimal, white and arbitrary environmental noise states are considered to demonstrate that the enhanced quantum illumination performs better in both parameter space and minimal error probability, just as we intuitively observed. A lower minimal error probability corresponds to a lower limit of the error probability of the one-shot event, *i.e.*, a higher detection accuracy. Our paper provides a new method that can improve the accuracy of illumination via the splitting process of high-energy particles, and its advantages are analyzed mathematically in detail. In particular, we deliberately control the two photons to form a detection unit in a fixed time interval, and the application potential of this temporal correlation is certainly far more than that.

The whole system of enhanced illumination is exhibited in the form of figure and formula derivation in the following sections. In our work, the HOM effect is demonstrated through the principle of the beam splitter (BS), which lays the theoretical foundation for the two-photon alignment of time in the radar transmitter. Superadd the optical alignment diagram of the transmitter path, then all of these researches will provide strong theoretical support for the feasibility of this scheme. Then the performance advantages of the enhanced detection unit in quantum illumination are analyzed in the framework of channel discrimination. The first part of the results mainly illustrates that the useful region in illumination parameter space is effectively expanded, and the second part mainly illustrates that the new detection unit has a lower minimal error probability than conventional illumination. In the results of these two parts, the white noise and arbitrary noise are analyzed respectively, and clear formula derivations and simulation results are given.

2. Methods

2.1. Transmitter design

HOM experiment is a classic work demonstrated by Hong, Ou, and Mandel in 1987,[17] which has the ability to measure the time interval between two-photon wave packets received one after another, and completely surpass the time resolution of the single photon counter.

The essence of the HOM effect is the destructive interference of two-photon probability amplitudes via the incidence of beams on both input sides of a 50:50 BS as shown in Fig. 1. If two photons enter into the BS through two input ports one after another severally, with their time interval longer than coherence time, the arrivals of two photons do not occur at the same time. At this time, these two photons will not interact with each other and will pass through the BS independently

by transmission or reflection, and the coincidence counting value can be observed between the two paths as well. If the incidences of two photons occur simultaneously, *i.e.*, the input state is $|1\rangle_0|1\rangle_1$, which is expressed in the Fock state, the photons then will blend and come out from either of the output sides of the BS with the same probability, rather than exiting from both sides severally. The output state can be written as

$$|\varphi_{\rm BS}\rangle = \frac{1}{\sqrt{2}}(|2\rangle_1|0\rangle_2 + |0\rangle_1|2\rangle_2). \tag{1}$$

To obtain the above-mentioned results, it is essential to conduct the standard quantum analysis of 50:50 BS. Out of the purpose of this work, only the special case where both photons arrive at the BS at the same time shall be discussed in detail. Each single reflection of the photon on the BS brings an extra $\pi/2$ to its phase, because of the fixed skewing $\exp(\pm i\pi/2) = \pm i$ between transmission and reflection. If the input state is the Fock state $|0\rangle_0|0\rangle_1$, apparently we obtain the output $|0\rangle_2|0\rangle_3$. If the input state is $|1\rangle_0|1\rangle_1 = \hat{a}_0^\dagger\hat{a}_1^\dagger|0\rangle_0|0\rangle_1$, where $\hat{a}_0^\dagger$ and $\hat{a}_1^\dagger$ correspond to the creation operator of input ports 0 and 1 respectively, and with the addition of $\hat{a}_0^\dagger = (\hat{a}_2^\dagger + i\hat{a}_3^\dagger)/\sqrt{2}$, $\hat{a}_1^\dagger = (i\hat{a}_2^\dagger + \hat{a}_3^\dagger)/\sqrt{2}$, the output state can be given by

$$\begin{aligned} |1\rangle_0|1\rangle_1 &\xrightarrow[\rm BS]{} \frac{1}{2}(\hat{a}_2^\dagger + i\hat{a}_3^\dagger)(i\hat{a}_2^\dagger + \hat{a}_3^\dagger)|0\rangle_2|0\rangle_3 \\ &= \frac{i}{2}(\hat{a}_2^\dagger\hat{a}_2^\dagger + \hat{a}_3^\dagger\hat{a}_3^\dagger)|0\rangle_2|0\rangle_3 \\ &= \frac{i}{\sqrt{2}}(|2\rangle_2|0\rangle_3 + |0\rangle_2|2\rangle_3). \end{aligned} \tag{2}$$

Clearly, at the output, there is no relative phase between $|2\rangle_2|0\rangle_3$ and $|0\rangle_2|2\rangle_3$. But inside the two-photon state, one will be reflected while the other passes through, that is to say, the output after the interference is in a two-photon state with a fixed $\pi/2$ relative phase inside.

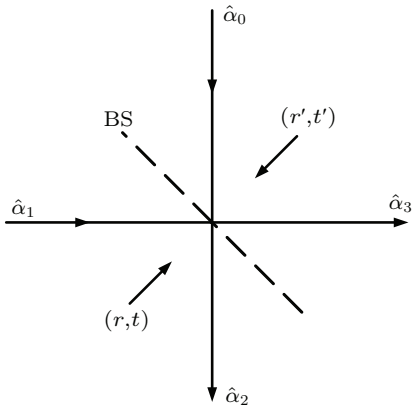


Fig. 1. Characteristic of the beam splitter.

To satisfy the commutation relation, the parameters above must meet the following conditions:

$$\begin{aligned} &|r'| = |r|, \quad |t'| = |t|, \quad |r|^2 + |t|^2 = 1, \\ &r^*t' + r't^* = 0, \quad r^*t + r't'^* = 0. \end{aligned} \tag{3}$$

Therefore, we design a radar transmitter as shown in Fig. 2. A laser device with a stable output wavelength of 405 nm is fabricated as an illuminant. When a beam of light of frequency $\omega_{\rm p}$ falls on a beta barium borate (BBO) crystal with 1–2 mm in length, some of the incident photons split into lower-frequency signal and idler photons at frequencies $\omega_{\rm s}$ and $\omega_{\rm i}$, where the subscripts "s" and "i" indicate "signal" and "idler" respectively.[56] It realizes an efficient generation of high-quality two photons that are non-collinear via the type-I SPDC process, and the lower-frequency photons have the same polarization which is perpendicular to the polarization of the pump. However, not all the spatial and temporal relations between two-photon pairs can be completely ascertained in practice, and the optical fiber of both roads cannot ensure the same length precisely. Nevertheless, the HOM interferometer can adjust the time interval between two photons to a fixed value *i.e.*, $\pi/2\omega_{\rm s}$ for the signal photon, which is too small to be measured by the single-photon counter. In the experiment, the two photons generated in the SPDC process are imported into the HOM interferometer, and the two-photons' coincidence count rate on the output paths is minimum by adjusting the position of the BS to make the two paths equal in length. At this time, beams in both optical roads are aligned for time with the fixed interval $\pm\pi/2\omega_{\rm s}$, which means that the detection of time-alignment two-photon can be recognized as one single counting. In other words, we can consider the two photons as a new probe unit, and also ensure that there are always two identical photons in each one-shot detection event. We move those single-photon counters away and regard the two optical output paths of the interferometer together as the output of the radar transmitter. So that the detection of a two-photon probe state emitted from the transmitter can be considered as a one-shot detection event stably.

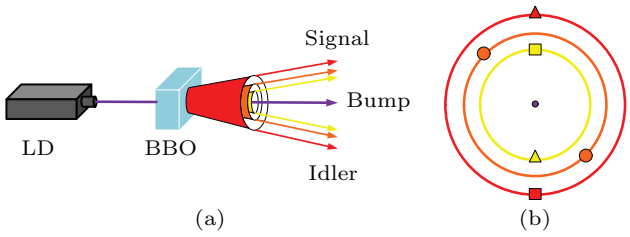


Fig. 2. Type-I SPDC process on BBO. (a) Pump light entering into a BBO crystal and the output consisting of several concentric emission cones. Various values of radius and colors correspond to different frequencies. (b) Sectional views of emission cones in panel (a). Light beams satisfying phase matching conditions are represented by the same marks, *e.g.*, circles, triangles, and squares. In this work, we are going to choose the pair of circles, denoting wavelength-degenerate signal and idler beams.

As shown in Fig. 2, different colors in the type-I SPDC process represent different frequencies of down-converted light, and the pairs of identical marks correspond to pairs of beams that satisfy the phase-matching condition $\omega_{\rm p} = \omega_{\rm s} + \omega_{\rm i}$ and $\boldsymbol{k}_{\rm p} = \boldsymbol{k}_{\rm s} + \boldsymbol{k}_{\rm i}$. In this experiment, we choose the degenerate scenario, *i.e.*, $\omega_{\rm s} = \omega_{\rm i} = \omega_{\rm p}/2$, which is denoted as circles

in Fig. 2(b). Then, the following is to import that pair of photons into the arms of the HOM interferometer and adjust the position of BS slightly to make these two optical paths have the same length. As mentioned in the previous section, the two photons' coincidence rate is a few percent of their median values in the wing, due to the destructive interference of probability amplitudes of two photons. And finally, the output of the HOM interferometer is collected and coupled into an optical fiber before the emission (see Fig. 3). At the receiver, positive-operator valued measure (POVM) measurements are performed on the photons received by the single photon counter to analyze the existence probability of the target. Therefore the measurement of quantum illumination can be seen as a problem of channel discrimination; two different channels correspond to the absence or presence of the target, and their input should be optimized to make the outputs most discriminable.

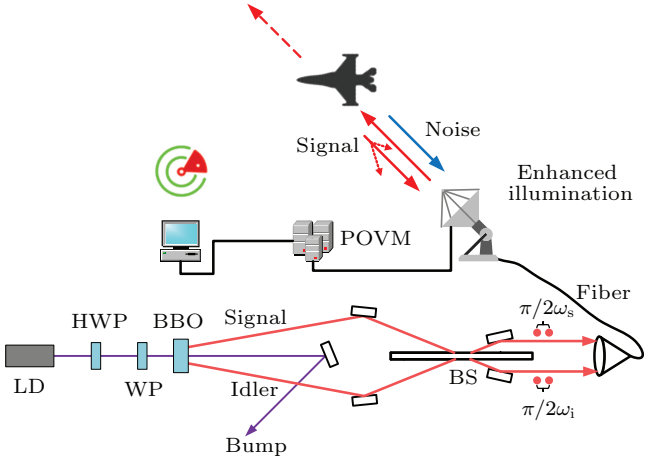


Fig. 3. Schematic diagram of radar transmitter and detection system.

In addition the materials and optical paths of the preparation for probe states are elaborately designed as shown in Figs. 2 and 3. In our setup, a pump laser beam at 405-nm pumps a type-I 2-mm-long BBO crystal that is cut for producing non-collinear degenerate emission. According to the two-photon spatial properties of parametric down conversion, the degenerate twin beams can be captured at symmetric positions in the far field around the degeneracy wavelength of 810 nm (see the pair of circles in Fig. 2(a)).[41,57] Then, a BS whose position is precisely adjusted ensures the conditions for the occurrence of destructive interference, *i.e.*, the same length of both optical paths for identical twin beams.[17] After the alignment process via the HOM interferometer, the enhanced probe unit consisting of two time-aligned photons is generated at both outputs of the BS and coupled into the single-mode fiber (810 nm) for emission. At this point, the degenerate probe state equation (2) has been prepared realistically. Moreover, the optimal POVM measurement operators (given in Subsection 2.2) are assumed to be used at the radar receiver to distinguish between signal and noise, so that the limit of error probability can be derived later.

2.2. Conventional and enhanced illumination

Following the frame of Ref. [22], where the signal is encoded with an optical photon mode and assuming that the thermal environment is at a temperature significantly lower than the optical energy, the received signal can be visible in the noise. Furthermore, we also assume that the radar receiver can perfectly distinguish a finite number of photonic modes of single photons. That is to say, the environment state can be approximately written as

$$\rho_{\rm th} \approx |{\rm vac}\rangle\langle{\rm vac}| + \sum_k O(\varepsilon)|1_k\rangle\langle 1_k| + O(\varepsilon^2), \tag{4}$$

where $|1_k\rangle$ denotes a single-photon state with frequency mode k.[10]

In this work, we pay attention to the one-shot part, which is a single detection event of the single-photon counter at the receiver of the radar. If we consider $\rho_{\rm th}$ shown above on the frequency basis with finite dimension d, then after triggering a one-shot event when the transmitter emits no signal photons, we can obtain the photon state at the receiver as

$$\rho_{\rm N} = \sum_{i=1}^{d} \lambda_i |\omega_i\rangle\langle\omega_i|. \tag{5}$$

That is a noise state with d kinds of possibilities in which each state $|\omega_i\rangle$ corresponds to a frequency mode whose possibility is λ_i and $\sum_{i=1}^{d}\lambda_i = 1$. In our radar setup, the frequency is set to be of single-mode, by using a red filter to ensure that the received photons are in an identical 810-nm frequency mode with a fixed bandwidth. The post-selected photons out of the red filter are sent to the measurement device and measured with the optimal POVM operators to discriminate signal photons from environment ones in polarization modes, which means $d = 2$. That is to say, the final noise we receive can be written as

$$\rho_{\rm N} = \lambda_1 |H\rangle\langle H| + \lambda_2 |V\rangle\langle V|, \tag{6}$$

where $|H\rangle$ and $|V\rangle$ denote horizontal polarization state and vertical polarization state respectively, and $\lambda_1+\lambda_2 = 1$. But for the sake of generality, we are going to perform the following derivations in frequency modes with Eq. (5).

For conventional illumination in one-shot detection, we transmit a single-photon state $\rho_{\rm s}$ to probe the distant targets and have two reception scenarios, ρ_0 and ρ_1.

2.2.1. ρ_0

As shown in Fig. 3, if the target is absent, the probe photon is completely lost, we can only receive photons from thermal noises. Thus the evolution of the photon state from radar transmitter to radar receiver is

$$\rho_{\rm S} \to \xi_0(\rho_{\rm s}) = \rho_{\rm N}. \tag{7}$$

2.2.2. ρ_1

if the target is present with probability η, which means that the single flight photon can be reflected by the target with probability η, and absorbed or scattered with probability $1-\eta$. Then the quantum state evolution is

$$\rho_{\rm s} \to \xi_1(\rho_{\rm s}) = \eta\rho_{\rm s} + (1-\eta)\rho_{\rm N}. \tag{8}$$

However, for the enhanced probe state emitted from our radar, two identical photons arrived at the receiver one by one with the invariable time interval $\pi/2\omega_{\rm s}$ can only trigger one single detection event, *i.e.* "one-shot". If one of the two photons is absorbed or scattered, the other photon can still finish the illumination process without any loss of accuracy, therefore, in a "one-shot" event, the two-photon state has one more chance to be detected . Therefore, this combination of identical photons can obviously increase the probability of signal reflection without changing the detection method. In this way, a scene where no signal photon arrives may occur with a probability of $(1-\eta)^2$, that is to say, we can describe the enhanced evolution situation of $\rho_{\rm s}$ as

$$\rho_{\rm s} \to \xi_{\rm e}(\rho_{\rm s}) = \left(2\eta-\eta^2\right)\rho_{\rm s} + (1-\eta)^2\rho_{\rm N}. \tag{9}$$

In this work, firstly, we simply approximate the background as white noise, *i.e.*, the values of λ_i for all $|\omega_i\rangle$ are identical so that equation (5) can be specified as

$$\rho_{\rm N} = \sum_{i=1}^{d} \frac{1}{d} |\omega_i\rangle\langle\omega_i|. \tag{10}$$

The final aim is to distinguish ρ_0 from ρ_1 with a minimum error probability via optimal input state and POVM measurement operators. Therefore, we construct a hypothesis testing model whose outcome is $Y=0$ for ρ_0 and $Y=1$ for ρ_1 to formulize the minimal error probability of measurement. The prior probability of ρ_0 is assumed to be p_0, thus the prior probability of ρ_1 is $p_1 = 1-p_0$. After POVM measurement operators $\{\boldsymbol{E}_0, \boldsymbol{E}_1\}$ are used to test which quantum state is given, one may make two mistakes of judgement: type-I error ('false alarm') $\rho_0 \xrightarrow[\text{test}]{E_1} Y=1$ and type-II error ('false negative') $\rho_1 \xrightarrow[\text{test}]{E_0} Y=0$ so that the error probability can be written as $P_{\rm error} = p_0\,{\rm tr}[\rho_0 E_1] + p_1\,{\rm tr}[\rho_1 E_0]$, which can be transformed into $P_{\rm error} = 1/2\{1-{\rm tr}[(p_0\rho_0 - p_1\rho_1)(E_0-E_1)]\}$. By denoting $\chi := p_0\rho_0 - p_1\rho_1$, χ can be decomposed by a set of orthonormal basis $\{|i\rangle\}$ into $\chi = \sum_i \alpha_i |i\rangle\langle i|$ with eigenvalue $\{\alpha_i\}$. According to the Helstrom theorem,[58] the optimal POVM is given by $E_0 = \sum_{\alpha_i \geq 0} |i\rangle\langle i|$ for the projector onto the positive support of χ; and $E_1 = \sum_{\alpha_i<0} |i\rangle\langle i|$ for the projector onto the negative support of χ. Thus the minimal error probability can be written as

$$P_{\rm error} = \frac{1}{2}\left(1 - \|p_0\rho_0 - p_1\rho_1\|\right), \tag{11}$$

where $\|\boldsymbol{A}\| = \sqrt{\boldsymbol{A}^\dagger \boldsymbol{A}}$ denotes the trace norm of matrix $\boldsymbol{A}$. To minimize the error probability, we must find out the optimal input state and POVM measurement to maximize the value $\|p_0\rho_0 - p_1\rho_1\|$, where $\rho_0 = \xi_0(\rho_{\rm s})$, $\rho_1 = \xi_1(\rho_{\rm s})$ and $\rho_{\rm e} = \xi_{\rm e}(\rho_{\rm s})$.

However, in optimizing the trace norm of the matrices over all possible density matrices, pure states prove to be capable of reaching the optimal result, so we only need to maximize the value $\|p_0\rho_0 - p_1\rho_1\|$ with the set of pure states.[10] In the background of the environment being a white noise state and for simplicity of calculation, we define $\Omega_{\rm c} = p_1\rho_1 - p_0\rho_0 = p_1\xi_1(\rho_{\rm s}) - p_0\xi_0(\rho_{\rm s})$, $P_{\rm error} = 1/2\left(1-\|\Omega_{\rm c}\|\right)$ for conventional illumination, and for enhanced illumination. Further $\Omega_{\rm c}$ and $\Omega_{\rm e}$ can be specified by the pure state input $|\varphi\rangle\langle\varphi| = |\omega_k\rangle\langle\omega_k|$ as

$$\begin{aligned}
\Omega_{\rm c} &= p_1\left(\eta|\varphi\rangle\langle\varphi| + (1-\eta)\left(\sum_{i=1}^{d}\frac{1}{d}|\omega_i\rangle\langle\omega_i|\right)\right) \\
&\quad - p_0\left(\sum_{i=1}^{d}\frac{1}{d}|\omega_i\rangle\langle\omega_i|\right) \\
&= p_1\eta|\varphi\rangle\langle\varphi| + \kappa\left(\sum_{i=1}^{d}\frac{1}{d}|\omega_i\rangle\langle\omega_i|\right), \\
\Omega_{\rm e} &= p_1\left(\left(2\eta-\eta^2\right)|\varphi\rangle\langle\varphi| + (1-\eta)^2\left(\sum_{i=1}^{d}\frac{1}{d}|\omega_i\rangle\langle\omega_i|\right)\right) \\
&\quad - p_0\left(\sum_{i=1}^{d}\frac{1}{d}|\omega_i\rangle\langle\omega_i|\right) \\
&= p_1\eta_{\rm e}|\varphi\rangle\langle\varphi| + \kappa_{\rm e}\left(\sum_{i=1}^{d}\frac{1}{d}|\omega_i\rangle\langle\omega_i|\right),
\end{aligned} \tag{12}$$

where $\kappa = p_1(1-\eta) - p_0$, $\kappa_{\rm e} = p_1(1-\eta)^2 - p_0$, $\eta_{\rm e} = 2\eta - \eta^2$. Thus

$$\begin{aligned}
\|\Omega_{\rm c}\| &= {\rm tr}\left(\sqrt{\Omega_{\rm c}^\dagger\Omega_{\rm c}}\right) = {\rm tr}\left(\sqrt{\left[p_1\eta|\varphi\rangle\langle\varphi| + \kappa\left(\sum_{j=1}^{d}\frac{1}{d}|\omega_j\rangle\langle\omega_j|\right)\right]\left[p_1\eta|\varphi\rangle\langle\varphi| + \kappa\left(\sum_{i=1}^{d}\frac{1}{d}|\omega_i\rangle\langle\omega_i|\right)\right]}\right) \\
&= {\rm tr}\left(\sqrt{(p_1\eta)^2|\omega_k\rangle\langle\omega_k| + \frac{2\kappa}{d}||\varphi\rangle|^2|\omega_k\rangle\langle\omega_k| + \frac{\kappa^2}{d^2}|\omega_k\rangle\langle\omega_k| + \kappa^2\sum_{i\neq k}^{d}\frac{1}{d^2}|\omega_i\rangle\langle\omega_i|}\right) \\
&= {\rm tr}\left(\left|p_1\eta + \frac{\kappa}{d}\right||\omega_k\rangle\langle\omega_k| + \sum_{i\neq k}^{d}\frac{|\kappa|}{d}|\omega_i\rangle\langle\omega_i|\right) = \left|p_1\eta + \frac{\kappa}{d}\right| + \frac{d-1}{d}|\kappa|.
\end{aligned} \tag{13}$$

Similarly, $\|\Omega_e\|$ for the enhanced two-photon state is given

$$\|\Omega_e\| = \left| p_1\eta_e + \frac{\kappa_e}{d} \right| + \frac{d-1}{d}|\kappa_e|. \tag{14}$$

3. Results

3.1. Expansion of useful parameter space

According to the equation derived above, the parameter space can be divided into three distinct regions, namely A, B, and C, by the positive and negative results for $p_1\eta + \kappa/d$ and κ. The comparison between conventional.[10] and enhanced illumination is shown below.

Region A: $p_0 \leq 1/2$ and $\kappa \geq 0$ $(\eta < 1 - p_0/p_1)$ for conventional illumination, $p_0 \leq 1/2$ and $\kappa_e \geq 0$ $(\eta < 1 - \sqrt{p_0/p_1})$ for enhanced illumination. Intuitionally $p_1\eta + \kappa/d \geq 0$ and $p_1\eta_e + \kappa_e/d \geq 0$, we can finally obtain the result $P_{\text{error}} = P^e_{\text{error}} = p_0$ a constant value, which means that it does not matter what the detection state is. That is to say, any pure state or mixed state can reach the bound as well. It seems that the received signal photons become useless for analyzing whether an object is present or not, due to the high prior probability of being present $p_1 > 1/2$ and low reflectivity η for the object. In this case, we always guess that the object is present to ensure the minimal error probability.

Region B: $p_0 > 1/2$ and $p_1\eta + \kappa/d < 0$ for conventional illumination, *i.e.*, $\eta < (p_0/p_1 - 1)(\lambda_i/(1-\lambda_i))$, and $p_1\eta_e + \kappa_e/d < 0$ for enhanced illumination, *i.e.*, $\eta_e < (p_0/p_1 - 1)(\lambda_i/(1-\lambda_i))$, where

$$\lambda_i = \frac{1}{d}, \quad \kappa < 0, \quad \kappa_e < 0. \tag{15}$$

And make $\eta_e = 2\eta - \eta^2$ and analyze η, then we will obtain

$$\begin{cases} \eta < 1 - \sqrt{1 - (p_0/p_1 - 1)(\lambda_i/(1-\lambda_i))}, & (p_0/p_1 - 1)(\lambda_i/(1-\lambda_i)) \leq 1, \\ \text{for all } \eta, & (p_0/p_1 - 1)(\lambda_i/(1-\lambda_i)) > 1 \end{cases} \tag{16}$$

for enhanced probe state. In this region, we can finally obtain the result $P_{\text{error}} = P^e_{\text{error}} = p_1$.

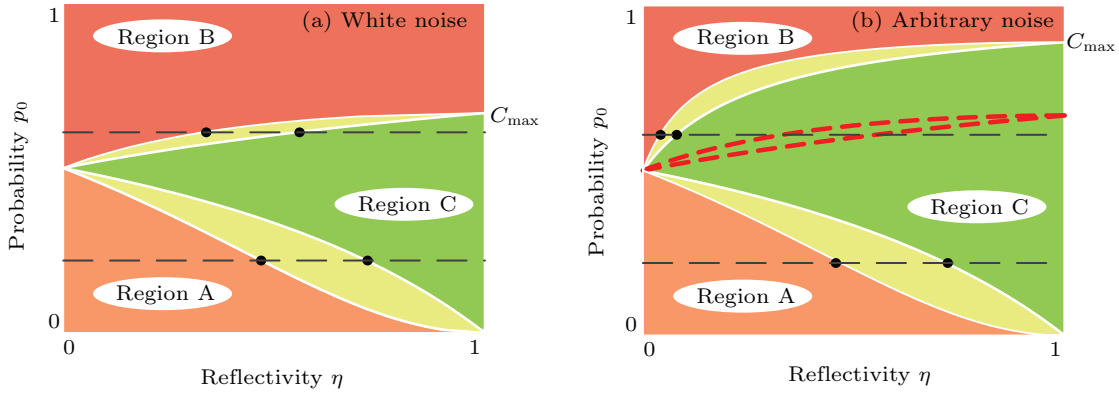


Fig. 4. Advantages of enhanced illumination over conventional illumination in different noise backgrounds. (a) In white noise background, the probability amplitudes of all the frequency bases are $1/d$, with the probe state being pure and the optimal POVM measurement being applied ultimately, the parameter space can be divided into region A, region B, and region C. The yellow parts denote the advantage of enhanced illumination. (b) In arbitrary noise background, we assume that the eigenvalues of the whole frequency basis follow decreasing sequence with $\sum_{i=1}^{d}\lambda_i = 1$, and the minimum eigenvalue $\lambda_d = 1/(4d)$, the red dotted lines in the figure correspond to the region B boundary of the conventional and enhanced situation in panel (a). Both measurements above are based on a polarized basis $\{|H\rangle, |V\rangle\}$, hence $d = 2$, and the yellow parts denote the advantage of enhanced illumination.

It is similar to region A, which means it does not matter what the probe state is, that is to say, any pure or mixed state can achieve the bound as well. We can explain this region as a regime, in which the received photons are useless for analysis due to the low reflectivity η. Therefore, we guess that the target is absent because of the high probability $p_0 > 1/2$, and minimal probability of making a wrong judgment is $P_{\text{error}} = P^e_{\text{error}} = p_1$.

Region C: the rest of the parameter space that satisfies the conditions $p_1\eta + \kappa/d \geq 0$ and $\kappa < 0$ for conventional illumination, and $p_1\eta + \kappa_e/d \geq 0$ and $\kappa_e < 0$ for enhanced illumination is named after region C. In this case, the minimal error probability is given by $P_{\text{error}} = p_1(1-\eta) + (2/d^2 - 1)\kappa$ for conventional illumination, and $P^e_{\text{error}} = p_1(1-\eta_e) + (2/d^2 - 1)\kappa_e$ for enhanced illumination.

As shown in Fig. 4(a), we call the regions A and B together a "guess region", where the probe photons are useless because only a few parts of the signal photons can be reflected and received successfully, then judgments have to be made simply with the prior probabilities p_0 and p_1. When the characteristic of the target is in region A or B, it means that the illumination radar will lose its function. On the contrary, the

larger region C makes the better adaptability of illumination radar to the target and the lower reflectivity limit of the target that can be detected so that reducing the area of guess region in parameter space is of great significance in improving the performance of illumination radar. In Fig. 4, comparing with the single-photon state, the upper and lower boundary of region C is expanded explicitly by the two-photon state, and the same p_0 on the new boundary of region C can tolerate a lower reflectivity η, which signifies a greater detection capability of radar for stealth objects with lower reflectivity. Even though we do not increase the maximum value of the analyzable region, *i.e.*, region C, we do accelerate the approximation of the upper and lower boundaries to a maximum value and minimum value as η increases, by improving the reflectivity of the stealth objects in a disguised form, and ultimately we realize an explicit promotion of the utilization efficiency of the parameter space.

3.2. Enhancement of minimal error probability

The comparison of minimal error probability between conventional[10] illumination and enhanced illumination is analyzed. As calculated in region A, *i.e.*, $p_0 < 0.5$, the conventional boundary $\eta < 1 - p_0/p_1$ is always larger than the enhanced boundary $\eta < 1 - \sqrt{p_0/p_1}$, except $p_0 = p_1$. And similarly in region B, the conventional boundary $\eta < (p_0/p_1 - 1)(\lambda_i/(1-\lambda_i))$ is always larger than the enhanced boundary $\eta < 1 - \sqrt{1-(p_0/p_1-1)(\lambda_i/(1-\lambda_i))}$, except $p_0 = p_1$. Therefore, as η increases, the value of enhanced minimal error probability starts to decline much earlier and remains lower than it in the conventional situation until $\eta = 1$, for both $p_0 < 0.5$ and $p_0 > 0.5$. However, as shown in Fig. 4, region C has a maximal value $C_{\max}$ on p_0 axis while $\eta = 1$. Therefore, the parameter of the target falls into region B, *i.e.*, the guess region when p_0 exceeds the level $C_{\max}$. From then on, signal photons become useless and the minimum error probability of the target is no longer affected by its reflectivity η, and it always equals p_1.

The calculation of performance advantage of the minimal error probability in the case of white noise has been completed. For the sake of generality, the characteristic of minimal error probability in the context of arbitrary noise whose spectrum $\lambda_1 \geq \lambda_2 \geq \lambda_3 \geq \cdots \geq \lambda_d$ is decreasingly ordered is also calculated next in detail. The performance advantages in both situations of noise are plotted in the same figure for comparison, with several cases of the prior probability p_0 enumerated [see Fig. 5]. Similar to the white noise, the division of parameter space of arbitrary noise remains unchanged, so we discuss the useful parameter space region C directly. Still, the pure state is inferred to be the optimal probe state. We assume that the probe state is the pure state $|\varphi\rangle = |\omega_i\rangle$, thus the $\Omega_{\rm c}$ can be written as

$$\Omega_{\rm c} = p_1\rho_1 - p_0\rho_0 = p_1\eta\,|\omega_k\rangle\langle\omega_k| + \kappa\sum_{i=1}^{d}\lambda_i\,|\omega_i\rangle\langle\omega_i|. \quad (17)$$

Then the trace norm of this operator is given by

$$\|\Omega_{\rm c}\| = {\rm tr}\sqrt{\left[(p_1\eta)^2 + 2\kappa\lambda_k + (\kappa\lambda_k)^2\right]|\omega_k\rangle\langle\omega_k| + \sum_{i\neq k}^{d}(\kappa\lambda_i)^2\,|\omega_i\rangle\langle\omega_i|} = |p_1\eta + \kappa\lambda_k| + (1-\lambda_k)\,|\kappa|\,. \quad (18)$$

While in region C, we obtain $p_1\eta + \kappa\lambda_k > 0$ and $\kappa < 0$, so that

$$\|\Omega_{\rm c}\| = p_1\eta + 2\kappa\lambda_k - \kappa. \quad (19)$$

Because of $\kappa < 0$, lower λ_k gives higher $\|\Omega_{\rm c}\|$, which means that the state $|\omega_d\rangle\langle\omega_d|$ corresponding to the minimum eigenvalue λ_d in the noise spectrum turns out to be the optimal probe state. After substituting $|\omega_d\rangle\langle\omega_d|$ into Eq. (18), we have

$$\|\Omega_{\rm c}\|_1 = p_1\eta + 2\kappa\lambda_d - \kappa, \quad (20)$$

$$P^{\rm a}_{\rm error} = \frac{1}{2}\left(1 - \|\Omega_{\rm c}\|_1\right), \quad (21)$$

where $\|\Omega_{\rm c}\|_1 = \max\left(\|\Omega_{\rm c}\left(|\varphi\rangle\langle\varphi|\right)\|\right)$. Using $\lambda_d = 1/d$ in white noise, and the unchanged constraint of the number of the dimension , the $\lambda_d = \min\left(\lambda_i\right)_{i=1}^{d}$ here definitely meets the condition $\lambda_d < 1/d$. Therefore, as a matter of course, a lower minimal error probability can be reached as long as we utilize the eigenstate corresponding to the minimum eigenvalue of the thermal environment as a probe state. As analyzed before, region A remains unchanged because of depending on nothing but p_0, thus the boundary between regions A and C does not change at all. However, the area of region B turns smaller with λ_d diminishing(see Fig. 4(b)).

The values of the minimum error probability and parameter space boundaries in two types of noise backgrounds for enhanced illumination and conventional illumination are illustrated in Fig. 5. Thereinto the boundary between regions A and C is called "region A boundary", and the boundary between regions B and C is named "region B boundary". When $p_0 < 0.5$, due to the enhanced $\eta_{\rm e}$ the region A boundary of enhanced illumination is always lower than that of conventional illumination, which corresponds to the downward extension of region C (see Fig. 4). When $p_0 = 0.5$, both boundaries are equal to 0. When $C_{\max} > p_0 > 0.5$, similar to the region A boundary, enhanced illumination brings about a lower region B boundary, which corresponds to the upward extension of region C (see Fig. 4). The advantage of the arbitrary noise situation is derived from its known noise spectrum, and then the minimum eigenvalue state can serve as the optimal probe

pure state, which provides a lower minimal error probability and the upward extension of region C only if $C_{\max} > p_0 > 0.5$ (see Fig. 4(b)). In other words, the probe pure state which has the lowest weight in the background noise spectrum gives the best performance of detection, not only for the probing accuracy but also for the radar applicability. Not to mention, when the enhanced illumination system is put into use, the performance of quantum illumination radar will reap a considerable improvement, especially for targets with low reflectivity. Furthermore, a lower detection error limit means that the probability of successfully detecting the target state in the radar detection process is greater, and the larger useful space undoubtedly renders radar more comprehensive and reliable in operational capability.

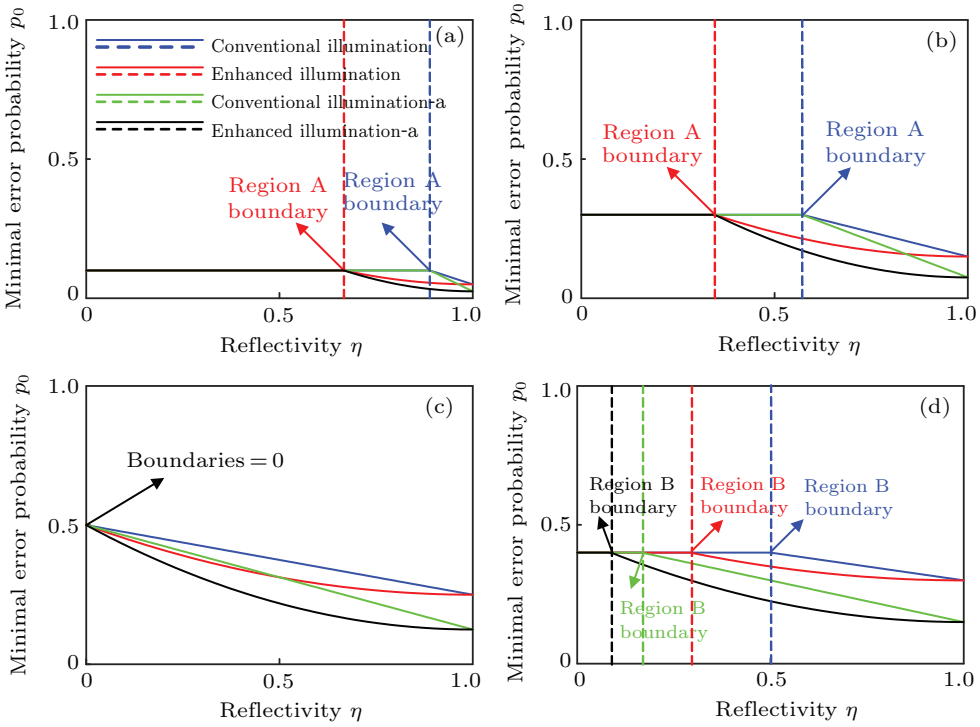


Fig. 5. Advantage of enhanced illumination in white noise and arbitrary noise background. Plots of minimal error probability *versus* reflectivity for prior probability $p_0 = 0.1$ (a), 0.3 (b), 0.5 (c), and 0.6 (d). In total region B $p_0 \geq 0.7$ and the minimal error probability is always p_1. The blue solid line and red solid line denote the variation of conventional illumination and enhanced illumination with η, respectively, in the white noise background. The green solid line and black solid line represent the variation of conventional illumination and enhanced illumination with η, respectively, in the arbitrary noise background. The dash lines correspond to the boundaries of regions A and B. As the signal is received after a filter whose central frequency is set to $\omega_p/2$, we discuss the simulation above with $d = 2$ and assumed $\lambda_d = 1/(4d)$, due to the two-dimensional basis $\{|H\rangle, |V\rangle\}$ of environmental noise.

4. Discussion

The transmitter designed above takes advantage of the type-I SPDC process on a nonlinear crystal, as is well known, pump photon whose frequency is ω_p splits into two lower-frequency photons only with a quite low probability. Particularly, after selecting phase-matching paired photons (signal and idler) from the output of crystal by using well-defined apertures and interference filters (IF) that are placed in the accurate position, there are fewer remaining photons which are available for the following interference. Despite this, we still cannot ensure the down-converted photons produced are precisely identical in practice since the substantial frequency spreads are hard to eliminate. Hence, the photon state out of the crystal should be written as $\int \mathrm{d}\omega \phi(\omega) |\omega_p/2+\omega\rangle |\omega_p/2-\omega\rangle$, where $\phi(\omega)$ denotes the weight function of ω and is peaked at $\omega = 0$. Theoretically, the coincidence rate falls to zero while the destructive interference occurs, however, because of a slight lack of overlap of the two photons' fields, the coincidence rate cannot always fall that far. The reason why we choose SPDC rather than two arbitrary beams of light is that the signal photons and the corresponding idler photons in the SPDC process are always generated simultaneously, so that the HOM interference takes place on each single pair of photons, which provides an enhanced light source with two photons aligned in time steadily and precisely. The vital difference between the enhanced illumination we put forward and the conventional illumination is that there are always two identical photons with fixed time intervals participating in each detection event.

5. Conclusions and perspectives

In this work, we proposed a brand new quantum illumination scheme and showed the elaborate design of the optical source, as well as its principle from the viewpoint of practical

experiments. Under the premise of optimal POVM measurement performed at the receiver, the performance of the proposed two-photon probe state is analyzed theoretically in detail under the famous illumination frame. The obtained results are explicit and forceful, as compared with the conventional method of single-photon detection. This time-aligned two-photon probe unit can greatly expand the proportion of useful area in parameter space, which reduces the dependence of quantum illumination radar in terms of the target prior knowledge and thus improving applicability. On condition that either prior knowledge or reflectivity of the target with strong capability of stealth is constant, compared with the conventional scheme, our scheme has an explicitly superior detection limit by means of its effective reduction of minimal error probability. Therefore, this radar transmitter can distinctly enhance the accuracy of illumination events, based on keeping the existing probing regime and receiving system unchanged. This strict time correlation also has great potential applications in quantum ranging and imaging, which can get rid of the time precision loss caused by clock alignment and obtain better imaging precision.

Acknowledgements

Project supported by the National Natural Science Foundation of China (Grant No. 62071363) and the Key Research and Development Program of Shaanxi Province, China (Grant No. 2021LLRH-06).

References

[1] Fan L and Zubairy M S 2018 *Phys. Rev. A* **98** 012319
[2] Lee S Y, Ihn Y S and Kim Z 2021 *Phys. Rev. A* **103** 012411
[3] Tan S H, Erkmen B I, Giovannetti V, Guha S, Lloyd S, Maccone L, Pirandola S and Shapiro J H 2008 *Phys. Rev. Lett.* **101** 253601
[4] Zhang S, Guo J, Bao W, Shi J, Jin C, Zou X and Guo G 2014 *Phys. Rev. A* **89** 062309
[5] Guha S and Erkmen B I 2009 *Phys. Rev. A* **80** 052310
[6] Kwiat P G, Mattle K, Weinfurter H, Zeilinger A, Sergienko A V and Shih Y 1995 *Phys. Rev. Lett.* **75** 4337
[7] Kwiat P G, Waks E, White A G, Appelbaum I and Eberhard P H 1999 *Phys. Rev. A* **60** R773
[8] Niu X L, Huang Y F, Xiang G Y, Guo G C and Ou Z 2008 *Opt. Lett.* **33** 968
[9] Roelofs M, Suna A, Bindloss W and Bierlein J 1994 *J. Appl. Phys.* **76** 4999
[10] Yung M H, Meng F, Zhang X M and Zhao M J 2020 *npj Quantum Information* **6** 75
[11] Banaszek K, U'Ren A B and Walmsley I A 2001 *Opt. Lett.* **26** 1367
[12] U'Ren A, Silberhorn C, Banaszek K, Walmsley I, Erdmann R, Grice W and Raymer M 2005 *Laser Physics* **15** 146
[13] Bennink R S 2010 *Phys. Rev. A* **81** 053805
[14] Wong F, Shapiro J and Kim T 2006 *Laser Physics* **16** 1517
[15] Louisell W, Yariv A and Siegman A 1961 *Phys. Rev.* **124** 1646
[16] Burnham D C and Weinberg D L 1970 *Phys. Rev. Lett.* **25** 84
[17] Hong C K, Ou Z Y and Mandel L 1987 *Phys. Rev. Lett.* **59** 2044
[18] Evans P G, Bennink R S, Grice W P, Humble T S and Schaake J 2010 *Phys. Rev. Lett.* **105** 253601
[19] Howell J C, Bennink R S, Bentley S J and Boyd R W 2004 *Phys. Rev. Lett.* **92** 210403
[20] Dada A C, Leach J, Buller G S, Padgett M J and Andersson E 2011 *Nat. Phys.* **7** 677
[21] Horodecki R, Horodecki P, Horodecki M and Horodecki K 2009 *Rev. Mod. Phys.* **81** 865
[22] Loudon R and Knight P L 1987 *J. Mod. Opt.* **34** 709
[23] O'brien J L 2007 *Science* **318** 1567
[24] Kitaev A Y, Shen A, Vyalyi M N and Vyalyi M N, 2002 *Classical and quantum computation* (American Mathematical Soc.)
[25] Gisin N, Ribordy G, Tittel W and Zbinden H 2002 *Rev. Mod. Phys.* **74** 145
[26] Buluta I and Nori F 2009 *Science* **326** 108
[27] Yung M H, Whitfield J D, Boixo S, Tempel D G and Aspuru-Guzik A 2014 *Quantum Information and Computation for Chemistry* pp. 67–106
[28] Bennett C H, Brassard G, Crépeau C, Jozsa R, Peres A and Wootters W K 1993 *Phys. Rev. Lett.* **70** 1895
[29] Giovannetti V, Lloyd S and Maccone L 2006 *Phys. Rev. Lett.* **96** 010401
[30] Cheung J, Chunnilall C, Woolliams E, Fox N, Mountford J, Wang J and Thomas P 2007 *J. Mod. Opt.* **54** 373
[31] Chang C S, Vadiraj A, Bourassa J, Balaji B and Wilson C 2019 *Appl. Phys. Lett.* **114** 112601
[32] Jonsson R, Di Candia R, Ankel M, Ström A and Johansson G 2020 *IEEE Radar Conference (RadarConf20)*. 2020, pp. 1–6
[33] Peshko I, Mogilevtsev D, Karuseichyk I, Mikhalychev A, Nizovtsev A, Slepyan G Y and Boag A 2019 *Opt. Express* **27** 29217
[34] Giovannetti V, Lloyd S and Maccone L 2001 *Nature* **412** 417
[35] Jacobson J, Björk G, Chuang I and Yamamoto Y 1995 *Phys. Rev. Lett.* **74** 4835
[36] Shapiro J H 2007 *Proceedings of SPIE 6603 Noise and Fluctuations in Photonics, Quantum Optics, and Communications*, June 7, 2007, Florence, Italy, p. 660306
[37] Brandt H E 1999 *Am. J. Phys.* **67** 434
[38] Lloyd S 2008 *Science* **321** 1463
[39] Wilde M M, Tomamichel M, Lloyd S and Berta M 2017 *Phys. Rev. Lett.* **119** 120501
[40] Zhuang Q, Zhang Z and Shapiro J H 2017 *JOSA B* **34** 1567
[41] Lopaeva E, Berchera I R, Degiovanni I P, Olivares S, Brida G and Genovese M 2013 *Phys. Rev. Lett.* **110** 153603
[42] De Palma G and Borregaard J 2018 *Phys. Rev. A* **98** 012101
[43] Harrow A W, Hassidim A, Leung D W and Watrous J 2010 *Phys. Rev. A* **81** 032339
[44] Bae J, Chruściński D and Piani M 2019 *Phys. Rev. Lett.* **122** 140404
[45] Piani M and Watrous J 2009 *Phys. Rev. Lett.* **102** 250501
[46] Sacchi M F 2005 *Phys. Rev. A* **72** 014305
[47] Sacchi M F 2005 *Phys. Rev. A* **71** 062340
[48] Clarke R B, Chefles A, Barnett S M and Riis E 2001 *Phys. Rev. A* **63** 040305
[49] Zhuang Q, Zhang Z and Shapiro J H 2017 *Phys. Rev. Lett.* **118** 040801
[50] Clerk A A, Devoret M H, Girvin S M, Marquardt F and Schoelkopf R J 2010 *Rev. Mod. Phys.* **82** 1155
[51] Lax M 1966 *Phys. Rev.* **145** 110
[52] Yan B, Giorgetti A and Paolini E 2021 *Signal Processing* **189** 108257
[53] Yan B, Paolini E, Xu N, Sun Z and Xu L 2021 *Signal Processing* **179** 107821
[54] Yan B, Paolini E, Xu L and Lu H M 2022 *IEEE Transactions on Geoscience and Remote Sensing*
[55] Pittman T B, Shih Y, Strekalov D and Sergienko A V 1995 *Phys. Rev. A* **52** R3429
[56] Wong F N C, Shapiro J H and Kim T 2006 *Laser Physics* **16** 1517
[57] Brida G, Degiovanni I P, Genovese M, Rastello M L and Ruo-Berchera I 2010 *Opt. Express* **18** 20572
[58] Helstrom C W 1969 *J. Stat. Phys.* **1** 231